Available online at www.sciencedirect.com
SCIENCE DIRECT®
International Journal of Solids and Structures 42 (2005) 2303–2322
INTERNATIONAL JOURNAL OF SOLIDS and STRUCTURES
www.elsevier.com/locate/ijsolstr

# Plasticity model using multiple failure criteria for concrete in compression

Honggun Park [a,*], Jae-Yo Kim [b,*]

[a] Department of Architecture, Seoul National University, San 56-1, Shinlim-Dong, Kwanak-Gu, Seoul 151-742, South Korea
[b] Research Institute of Technology, Samsung Engineering and Construction, Seohyun Building, 270-1, Seohyun-Dong, Bundang-Gu, Sungnam-Si, Gyonggi-Do, 463-771, South Korea

Received 6 February 2004; received in revised form 18 September 2004
Available online 2 November 2004

**Abstract**

A plasticity model was developed to predict the behavioral characteristics of concrete in multiaxial compression. To extend the applicability of the plasticity model to concrete in various stress states, a new model that uses multiple failure criteria was attempted. A stress was decomposed into one volumetric and two deviatoric components orthogonal to each other. Independent failure criterion was provided for each stress component. To satisfy the three failure criteria, the plasticity model using multiple failure criteria was implemented. To describe dilatancy due to compressive damage, a non-associative flow rule was proposed. The proposed model was compared with various existing test results. The comparisons show that it predicted most of the experimental results well by applying the three independent failure criteria.


*Keywords:* Plasticity; Concrete; Compression; Finite element analysis; Failure criteria

## 1. Introduction

For nonlinear analysis of concrete, various material models—plasticity models, damage models, damage-plasticity models, microplane models, and so on—have been developed. Based on numerous theoretical studies and test results, these models have been used to accurately describe the behavioral characteristics of concrete in various compressive stress states.

* Corresponding authors. Tel.: +82 2 880 7055/7053; fax: +82 2 871 5518.
*E-mail addresses:* parkhg@snu.ac.kr (H. Park), jyo.kim@samsung.com (J.-Y. Kim).

0020-7683/$ - see front matter © 2004 Elsevier Ltd. All rights reserved.
doi:10.1016/j.ijsolstr.2004.09.029

Concrete shows various behavioral characteristics depending on its stress states. In uniaxial compression, the initial response is almost linear, and as the compressive stress reaches its maximum, microcracking causes concrete to behave nonlinearly. In the post-peak behavior, the concrete volume increases because of the unstable propagation of the microcracks. In biaxial compression, Kupfer et al. (1969) reported that maximum strength of concrete increases up to 125% of the uniaxial strength depending on the ratio of the two orthogonal stresses. Comparable strength enhancement was also confirmed in other biaxial compression tests (Liu et al., 1972; Nelissen, 1972; Tasuji et al., 1978). In triaxial compression tests (Kotsovos and Newman, 1978; Wang et al., 1987; Smith et al., 1989; Bellotti and Rossi, 1991; Xie et al., 1995; Imran and Pantazopoulou, 1996; Li and Ansari, 1999; Sfer et al., 2002), the strength and ductility of concrete significantly increase due to the confinement effect (Fig. 1).

To describe these behavioral characteristics of concrete in compression, the plasticity model was frequently used because of its simple and direct representation of multiaxial stress. Since Chen and Chen (1975), many researchers have attempted to extend the application of the plasticity model to various stress states of concrete. To predict concrete strength in various stress states, several failure criteria defined with stress invariants were developed: the 3-parameter criterion (Willam and co-workers), 4-parameter criterion (Ottosen, Hsieh-Ting-Chen), 5-parameter criterion (Willam–Warnke), and others (Chen, 1982; Menetrey and Willam, 1995). Also, to describe deformational characteristics of concrete in ultimate stress state, various non-associative flow rules were developed (Pramono and Willam, 1989; Kang and Willam, 1999; Imran and Pantazopoulou, 2001; Grassl et al., 2002).

With these sophisticated failure criteria and the flow rule, recent plasticity models have described well the behavior of concrete in multiaxial compression (Imran and Pantazopoulou, 2001; Grassl et al., 2002). However, existing plasticity models using a single failure criterion is limited in describing the complex behavioral characteristics of concrete. Single failure criterion and the corresponding plastic strain are not sufficient to accurately describe the complex behavior of concrete varying according to the stress combinations. Usually, their application is limited to test data used for calibrations of the models. For good agreement with other test results, the parameters used in the existing plasticity models should be adjusted. Therefore, a new model which is able to predict various test results without adjustment of other variables except the basic variables such as the uniaxial compressive strength and the corresponding strain is needed to extend the applicability of the plasticity model.

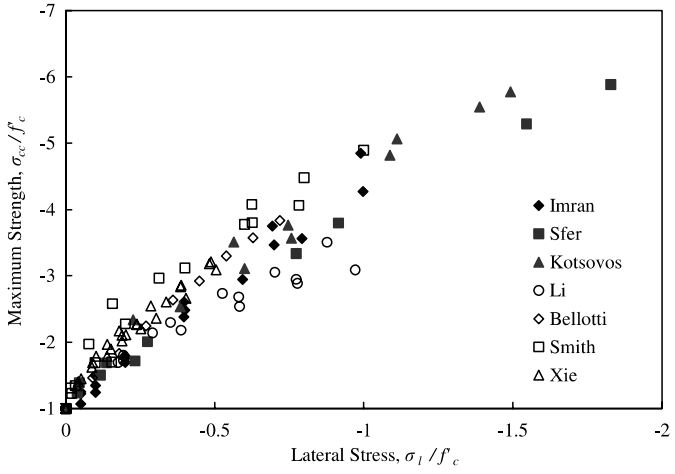


Fig. 1. Test results—triaxial compression.

Bazant and co-workers developed the microplane model to overcome such disadvantages of the plasticity model (Bazant and Prat, 1988a). In the microplane model, the macroscopic stress representing a spherical volume of concrete is calculated by integrating the volumetric, deviatoric, and tangential microscopic stresses defined in the microplanes composing the spherical surface. Numerical calculations can be easily performed due to the simple microscopic stress–strain relations. Various behavioral characteristics of concrete can be accurately described by the combination of the microscopic stress–strain relations defined in multi-oriented microplanes. The accuracy of the microplane model confirms that independent stress–strain relationships should be applied to the decomposed volumetric, deviatoric, and tangential components. However, the microplane model has several shortcomings: The orientation of the tangential stress component is not clearly defined; variables still need to be adjusted for several tests; and the specific strength of concrete intended might not be predicted exactly because various stress–strain relations defined in the multi-oriented microplanes are used in calculating the macroscopic stress.

In the present study, incorporating the advantages of the microplane model, a plasticity model was developed to describe the behavioral characteristics of concrete in various compressive stress states. The decomposition of volumetric and deviatoric components and the related formulations used in the microplane model were introduced in the framework of the plasticity theory.

## 2. Definition of stress components

For a stress tensor $\sigma_{ij}$, stress invariants are defined as $I_1 = \delta_{ij}\sigma_{ij}$, $J_2 = s_{ij}s_{ij}/2$, and $J_3 = s_{ij}s_{jk}s_{ki}/3$. $s_{ij}$ is the deviatoric stress tensor: $s_{ij} = \sigma_{ij} - \sigma_{kk}\delta_{ij}/3$. $\delta_{ij}$ is the Kronecker symbol defined as $\delta_{ij} = 1$ if $i = j$ and $\delta_{ij} = 0$ if $i \neq j$. Figs. 2 and 3 show stress components defined in the principal stress space and deviatoric plane, respectively. In the figures, $\sigma_1 > \sigma_2 > \sigma_3$, where principal compressive stresses $\sigma_1$, $\sigma_2$, and $\sigma_3$ are negative. In general, a stress is represented by the hydrostatic stress invariant $\xi$, the deviatoric stress invariant $\rho$, and the deviatoric polar angle $\theta$, which are defined with stress invariants: $\xi = I_1/\sqrt{3}$, $\rho = \sqrt{2J_2}$, and $\cos 3\theta = (3\sqrt{3}J_3)/(2J_2^{3/2})$. $\theta = \pi/3$ represents the uniaxial compressive stress and $\theta = 0$ represents the equal biaxial compression. The hydrostatic stress invariant $\xi$ is an important index which determines the enhancement of strength and ductility in multiaxial compression.

In the present study, unlike the general definition mentioned, a compressive stress is presented with three orthogonal components. The proposed approach is similar to the microplane model in that a stress is

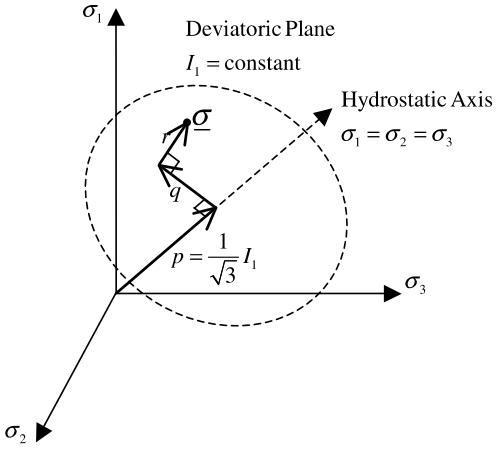


Fig. 2. Stress components in principal stress space.

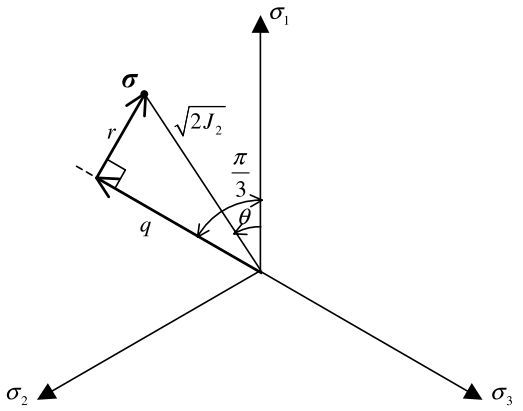


Fig. 3. Stress components in deviatoric plane.

decomposed into three independent stresses. The three components $p$, $q$, and $r$ used in the proposed model are defined as (see Figs. 2 and 3):

$$p = |I_1/\sqrt{3}| \tag{1a}$$

$$q = |\sqrt{2J_2}\cos(\pi/3 - \theta)| \tag{1b}$$

$$r = |\sqrt{2J_2}\sin(\pi/3 - \theta)| \tag{1c}$$

A stress vector is defined by the combination of three independent vectors related to $p$, $q$, and $r$ ($0 \geqslant \sigma_1 \geqslant \sigma_2 \geqslant \sigma_3$):

$$(\sigma_1, \sigma_2, \sigma_3) = p\left(-\frac{1}{\sqrt{3}}, -\frac{1}{\sqrt{3}}, -\frac{1}{\sqrt{3}}\right) + q\left(\frac{1}{\sqrt{6}}, \frac{1}{\sqrt{6}}, -\frac{1}{\sqrt{6}}\right) + r\left(\frac{1}{2}, -\frac{1}{2}, 0\right) \tag{2}$$

Component $p$ is identical to the hydrostatic stress invariant $\xi$ representing the volumetric part, and affects the enhancement of strength and ductility in multiaxial compression. Components $q$ and $r$ representing the deviatoric part are related to the deviatoric stress invariant $\rho$ and the deviatoric polar angle $\theta$. Component $q$ presents behavioral characteristics of concrete in uniaxial compression, and is identical to the deviatoric stress invariant $\rho$ in uniaxial compression ($\theta = \pi/3$). Component $r$ presents behavioral characteristics of concrete in biaxial or triaxial compression and reaches the maximum value in equal biaxial compression ($\theta = 0$).

As such, a compressive stress is composed of three components representing behavioral characteristics of concrete in uni-, bi-, and triaxial compressions. The behavioral characteristics of concrete were already clarified through existing experimental and theoretical studies (Chen, 1982; Bazant and Prat, 1988a,b). Therefore, three orthogonal components $p$, $q$, and $r$ can be clearly defined to describe such behavioral characteristics of concrete.

## 3. Failure criteria

As mentioned, a stress is composed of three orthogonal components—one volumetric and two deviatoric components—and the independent failure criteria are applied on these three stress components. To apply these multiple failure criteria, the plasticity model, previously developed by Park and Klingner (1997), was

modified. In the proposed plasticity model, three independent failure criteria for the orthogonal components must be satisfied:

$$f_1 = f_2 = f_3 = 0 \tag{3}$$

where subscripts '1', '2', and '3' indicate the orthogonal components $p$, $q$, and $r$, respectively. Total plastic strain vector $\underline{\varepsilon}_p$ is defined as the sum of the plastic strain vectors $\underline{\varepsilon}_{pi}$ related to the corresponding failure criteria: $\underline{\varepsilon}_p = \sum_i^3 \underline{\varepsilon}_{pi}$.

The failure criteria are defined as

$$f_1 = \hat{\sigma}_1(I_1) - \overline{\sigma}_1(\hat{\varepsilon}_{p1}) = 0 \tag{4a}$$

$$f_2 = \hat{\sigma}_2(J_2, J_3) - \overline{\sigma}_2(\hat{\varepsilon}_{p1}, \hat{\varepsilon}_{p2}) = 0 \tag{4b}$$

$$f_3 = \hat{\sigma}_3(J_2, J_3) - \overline{\sigma}_3(\hat{\varepsilon}_{p1}, \hat{\varepsilon}_{p3}) = 0 \tag{4c}$$

where $\hat{\sigma}_i$ is the effective stress defined with stress invariants and $\overline{\sigma}_i$ is the failure surface function defined by a function of equivalent plastic strain $\hat{\varepsilon}_{pi}$. Each effective stress is identical to the stress component $p$, $q$, or $r$ defined in Eq. (1).

$$\hat{\sigma}_1(I_1) = |I_1/\sqrt{3}| \tag{5a}$$

$$\hat{\sigma}_2(J_2, J_3) = |\sqrt{2J_2}\cos(\pi/3 - \theta)| \tag{5b}$$

$$\hat{\sigma}_3(J_2, J_3) = |\sqrt{2J_2}\sin(\pi/3 - \theta)| \tag{5c}$$

The effective stress $\hat{\sigma}_1$ represents the hydrostatic stress, and $\hat{\sigma}_2$ and $\hat{\sigma}_3$ represent the deviatoric stress defined in the deviatoric plane.

$\overline{\sigma}_1$, $\overline{\sigma}_2$, and $\overline{\sigma}_3$ present the failure surfaces for the corresponding effective stresses. According to existing test results, an increase in the hydrostatic stress induces the expansion of the failure surface in the deviatoric plane. Fig. 4 shows $\xi$–$\rho$ relations obtained from laterally confined triaxial compression tests ($\theta = \pi/3$), and their average compressive meridian. As shown in the figure, the failure surface linearly increases in low hydrostatic stress, but its increasing rate decreases in high hydrostatic stress. This is also observed in Fig. 1 showing the variations of the maximum compressive strength according to the lateral confining stress. The failure surface for the hydrostatic part $\overline{\sigma}_1$ in Eq. (4a) can be defined by the volumetric equivalent

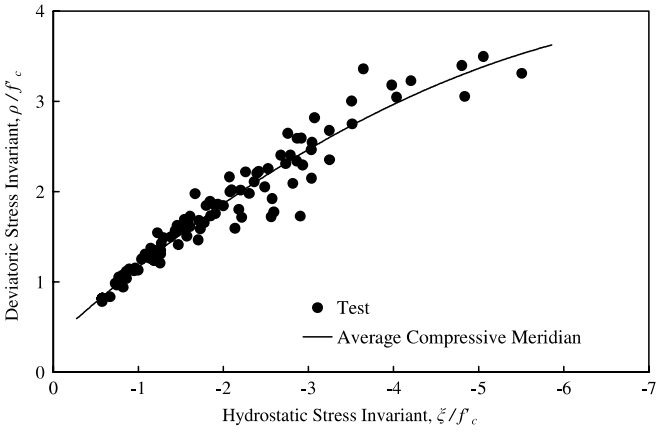


Fig. 4. Test results in $\xi$–$\rho$ plane.

plastic strain $\hat{\varepsilon}_{p1}$. On the other hand, to describe dependency of the failure surface on hydrostatic stress, the failure surfaces for the deviatoric part $\overline{\sigma}_2$ and $\overline{\sigma}_3$ in Eqs. (4b) and (4c) should be defined by the volumetric equivalent plastic strain $\hat{\varepsilon}_{p1}$ as well as the deviatoric equivalent plastic strains $\hat{\varepsilon}_{p2}$ and $\hat{\varepsilon}_{p3}$.

## 4. Definition of failure surface

In the classical plasticity theory, the yield surface is defined, and plastic deformation begins to develop after a stress reaches the yield surface. In the proposed model, the elastic and plastic regions are not separated and continuous transition of failure surfaces defined with equivalent plastic strains is assumed to occur from the initial loading. Failure surfaces $\overline{\sigma}_i$ are defined by the same functions as used for the volumetric and deviatoric stress–strain relations in the microplane model (Bazant and Prat, 1988b). In the proposed model, the failure surface functions are defined with the equivalent plastic strains rather than the microscopic strains (Fig. 5).

$$\frac{\overline{\sigma}_1}{f'_c} = \frac{E_c}{1-2v}\left[\left(1+\frac{\hat{\varepsilon}_{p1}}{a}\right)^{-s} + \left(\frac{\hat{\varepsilon}_{p1}}{b}\right)^{t}\right]\hat{\varepsilon}_{p1} \tag{6a}$$

$$\frac{\overline{\sigma}_2}{f'_c} = \frac{E_c}{1+v}\exp\left[-\left(\frac{\hat{\varepsilon}_{p2}}{c_2}\right)^{m_2}\right]\hat{\varepsilon}_{p2} \tag{6b}$$

$$\frac{\overline{\sigma}_3}{f'_c} = \frac{E_c}{1+v}\exp\left[-\left(\frac{\hat{\varepsilon}_{p3}}{c_3}\right)^{m_3}\right]\hat{\varepsilon}_{p3} \tag{6c}$$

Coefficients used in the failure surface functions were determined based on various test results. Since failure surface $\overline{\sigma}_1$ is related to the hydrostatic stress, coefficients in $\overline{\sigma}_1$ were determined from the results of the hydrostatic triaxial test (Green and Swanson, 1973): $a = 2.5\times10^{-5}$, $b = 2.5$, $s = 0.8$, and $t = 1.15$. These

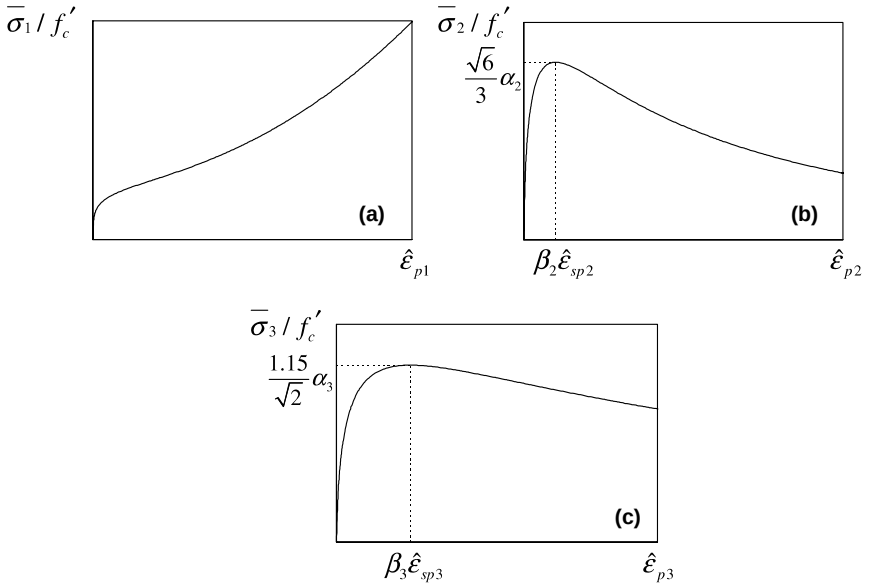


Fig. 5. Failure surfaces: $\overline{\sigma}_1$, $\overline{\sigma}_2$, and $\overline{\sigma}_3$.

values are also valid for other hydrostatic triaxial tests. Since failure surface $\overline{\sigma}_2$ is related mainly to uniaxial compressive stress, coefficients used in $\overline{\sigma}_2$ were determined with uniaxial compressive strength and the corresponding strain: In uniaxial compression, when a stress reaches the maximum strength $f'_c$, the effective stress $\hat{\sigma}_2$ becomes $\sqrt{6}f'_c/3$ (see Eq. (2)), which should be the maximum of $\overline{\sigma}_2$ (Fig. 5(b)). Using this condition, the coefficients in Eq. (6b) are defined as

$$m_2 = -\frac{1}{\ln\left(\frac{(1+\nu)}{E_c}\frac{\sqrt{6}}{3}\frac{\alpha_2}{\beta_2\hat{\varepsilon}_{sp2}}\right)} \tag{7a}$$

$$c_2 = \beta_2\hat{\varepsilon}_{sp2}(1/m_2)^{1/m_2} \tag{7b}$$

$\alpha_2$ and $\beta_2$ are the magnification factors representing enhanced strength and ductility of concrete in multiaxial compression, respectively. In uniaxial compression, $\alpha_2 = \beta_2 = 1$. The value of $\hat{\varepsilon}_{sp2}$, which is the equivalent plastic strain corresponding to the maximum uniaxial compressive strength, was set to 0.0012 based on the results of uniaxial compression test (Kupfer et al., 1969).

In the same manner, coefficients used in failure surface $\overline{\sigma}_3$ were determined using maximum strength in equal biaxial compression $1.15f'_c$ (Kupfer et al., 1969).

$$m_3 = -\frac{1}{\ln\left(\frac{(1+\nu)}{E_c}\frac{1.15}{\sqrt{2}}\frac{\alpha_3}{\beta_3\hat{\varepsilon}_{sp3}}\right)} \tag{8a}$$

$$c_3 = \beta_3\hat{\varepsilon}_{sp3}(1/m_3)^{1/m_3} \tag{8b}$$

$\alpha_3$ and $\beta_3$ are the magnification factors representing enhanced strength and ductility of concrete in multiaxial compression, respectively. In equal biaxial compression, $\alpha_3 = \beta_3 = 1$. The value of $\hat{\varepsilon}_{sp3}$ corresponding to the maximum strength in equal biaxial compression was set to 0.0025 based on the results of biaxial compression test (Kupfer et al., 1969).

A concrete shows enhanced strength and ductility in multiaxial compression, particularly in triaxial compression. Based on recent test results for triaxial compression, Imran and Pantazopoulou (2001) proposed the formula for laterally confined compressive strength by modifying the Hsieh-Ting-Chen failure criterion.

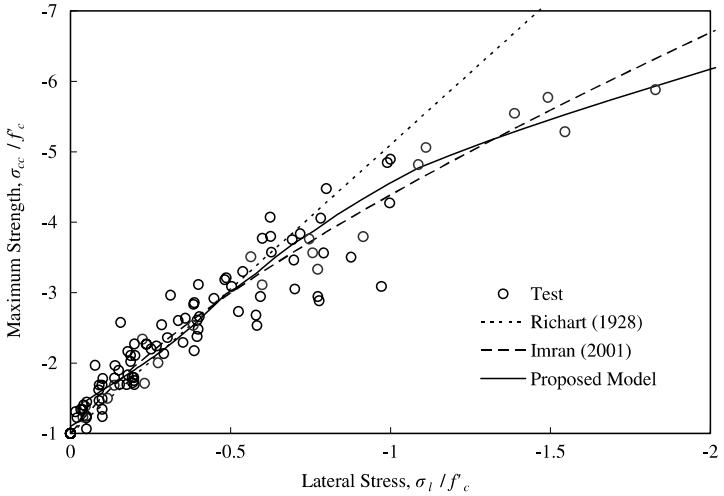


Fig. 6. Comparison of proposed strength equations and test results.

$$\frac{\sigma_{cc}}{f'_c} = \frac{\sigma_l}{f'_c} + 0.021 - \sqrt{1.043 - 10.571\frac{\sigma_l}{f'_c}} \tag{9}$$

where $\sigma_l$ is the confining compressive stress orthogonal to the maximum principal compressive stress ($\sigma_3 < \sigma_2 = \sigma_1 (= \sigma_l) < 0$), and $\sigma_{cc}$ is the compressive strength enhanced by the confining compressive stress (if $\sigma_l = 0$, $\sigma_{cc} = -f'_c$). As shown in Fig. 6, Eq. (9) agrees relatively well with test results for various compressive strengths and lateral confining stresses. In the present study, based on Eq. (9), a formula addressing the confining effect was derived.

Unlike the traditional plasticity models, in the proposed model, the confining effect was presented in the failure surface function rather than in the effective stress. For this, the function for the confining effect should be defined by the volumetric plastic strain rather than the hydrostatic stress (lateral confining stress) (Fig. 7). Based on the results of laterally confined triaxial compression test (Kotsovos and Newman, 1978; Smith et al., 1989; Bellotti and Rossi, 1991; Xie et al., 1995; Imran and Pantazopoulou, 1996; Li and Ansari, 1999; Sfer et al., 2002), the enhanced strength in multiaxial compression was defined as

$$\frac{\sigma_{cc}}{f'_c} = -1 - 0.575(K\hat{\varepsilon}_{p1} - 0.45)^{0.315} \tag{10}$$

where $K(=E_c/3(1-2\nu))$ is the bulk modulus. From Eq. (10), the strength magnification factor $\alpha_2$ in Eq. (7) was defined as

$$\alpha_2 = 1 + 0.575(K\hat{\varepsilon}_{p1} - 0.45)^{0.315} \tag{11}$$

Fig. 6 compares the analytical results by Eq. (11) with test results. The analytical results obtained using $E_c = 29{,}000$ MPa and $\nu = 0.15$ agree well with the test results.

Similarly, the strain magnification factor $\beta_2$ was defined as

$$\beta_2 = 1 + 8.4(K\hat{\varepsilon}_{p1} - 0.45)^{0.25} \tag{12}$$

Eq. (12) was determined by comparisons with the laterally confined triaxial tests (Kotsovos and Newman, 1978; Smith et al., 1989; Bellotti and Rossi, 1991; Xie et al., 1995; Imran and Pantazopoulou, 1996; Li and Ansari, 1999; Sfer et al., 2002). In this equation, the enhancement of ductility due to hydrostatic stress is described indirectly by the function of equivalent volumetric strain.

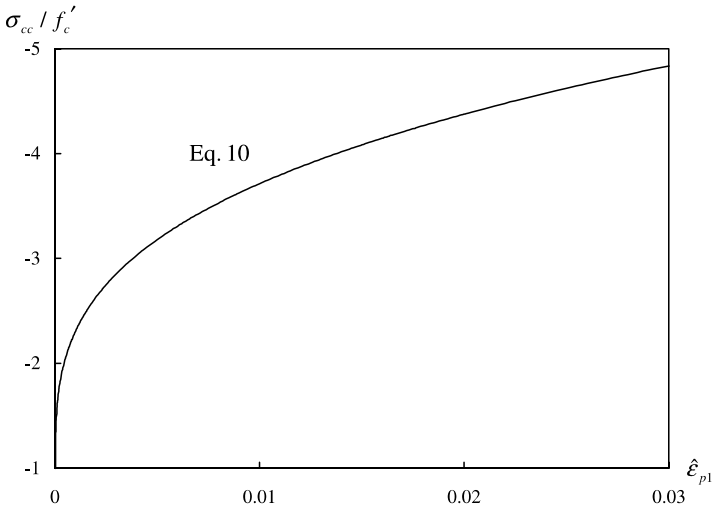


Fig. 7. Strength enhancement vs equivalent volumetric plastic strain.

Based on the results of triaxial compression tests by Wang et al. (1987), the strength magnification factor $\alpha_3$ and the strain magnification coefficient $\beta_3$ for the failure surface $\overline{\sigma}_3$ were defined as

$$\alpha_3 = 1 + 0.389(K\hat{\varepsilon}_{p1} - 2.17)^{0.315} \tag{13}$$

$$\beta_3 = 1 + 5.95(K\hat{\varepsilon}_{p1} - 2.17)^{0.25} \tag{14}$$

As mentioned, magnification factors $\alpha_2$, $\alpha_3$, $\beta_2$, and $\beta_3$ for the deviatoric part were determined only by the equivalent volumetric plastic strain $\hat{\varepsilon}_{p1}$. The enhancement in strength and ductility of concrete due to multiaxial compression is described by the failure surfaces defined with these coefficients. In the proposed model, only the basic properties of concrete—uniaxial compressive strength, elastic modulus, and Poisson's ratio—will be used in predicting the test results, without arbitrarily adjusting other coefficients.

## 5. Plastic strain

Plastic strains are defined by the gradient of the plastic potential function, and the related rule is defined as the plastic flow. Results of the uniaxial and multiaxial compressive tests clearly show non-association characteristics of the volumetric strain (Smith et al., 1989; Sfer et al., 2002). In the test results, the volumetric part of the plastic strain rapidly changes from contraction to dilatation as the compressive damage of concrete progresses and strength softening occurs after the peak stress. The associative flow rule defining the volumetric strain proportionally to the hydrostatic stress cannot describe the dilatation due to compressive damage. Existing plasticity models use various non-associative flow rules (Pramono and Willam, 1989; Kang and Willam, 1999; Imran and Pantazopoulou, 2001; Grassl et al., 2002). In the present study, a simple form of the non-associative flow is proposed.

As shown in Fig. 5, the volumetric function presents continuously increasing stress. This means that the compressive damage of concrete and the resulting decrease in compressive stress occur due to softening of the deviatoric stresses. The softening of deviatoric stress is accompanied by significant increase in the deviatoric equivalent plastic strain. Thus, to describe the increase in the volumetric strain due to compressive damage, the volumetric plastic strain should be related to the deviatoric equivalent plastic strain.

For this purpose, the plastic potentials used to define plastic strains are defined as

$$g_1 = f_1 \tag{15a}$$

$$g_2 = \kappa f_1 + f_2 \tag{15b}$$

$$g_3 = \kappa f_1 + f_3 \tag{15c}$$

The volumetric plastic potential $g_1$ is identical to the first failure criterion $f_1$. To relate the deviatoric equivalent plastic strain to the volumetric strain, the deviatoric plastic potentials $g_2$ and $g_3$ are defined as linear combinations of the failure criteria for the volumetric part and the deviatoric part. Based on the results of various compression tests (Kupfer et al., 1969; Tasuji et al., 1978; Kotsovos and Newman, 1978; Imran and Pantazopoulou, 1996; van Mier, 1986), coefficient $\kappa$ was defined as the ratio of the deviatoric to hydrostatic invariants: $\kappa = -J_2/I_1^2$.

Based on the proposed non-associative flow rule, incremental plastic strain vector for each failure criterion is defined as

$$\mathrm{d}\underline{\varepsilon}_{pi} = \mathrm{d}\lambda_i \left(\frac{\partial g_i}{\partial \underline{\sigma}}\right) \tag{16}$$

where $d\lambda_i$ = incremental plastic strain multiplier. Incremental equivalent plastic strain $d\hat{\varepsilon}_{pi}$ is defined with the incremental plastic strain vector.

$$d\hat{\varepsilon}_{pi} = [(2/3)(d\underline{\varepsilon}_{pi} \cdot d\underline{\varepsilon}_{pi})]^{1/2} = C_i d\lambda_i \tag{17}$$

where $C_i$ = equivalent plastic potential gradient, and $d\lambda_i$ = incremental plastic strain multiplier. Total equivalent plastic strain $\hat{\varepsilon}_{pi}$ is defined as the sum of the incremental equivalent plastic strain $d\hat{\varepsilon}_{pi} : \hat{\varepsilon}_{pi} = \int d\hat{\varepsilon}_{pi}$.

By using Eqs. (15b), (15c), (16) and (17), the increase in the equivalent deviatoric plastic strains causes dilatation (minus increase in volumetric plastic strain).

## 6. Numerical calculation

In nonlinear finite element analyses, it is necessary to obtain the current stress satisfying all the failure criteria in Eq. (4) for given total strains or strain increments. In a plasticity model, stresses satisfying all the failure criteria for given strains cannot be directly calculated. Therefore, a typical elastic-predictor–plastic-corrector algorithm, in which the stresses for given strains are obtained by iterative calculations with initially predicted stresses in each load step, was applied in the present study (Crisfield, 1991; Park and Klingner, 1997). For the iterative procedure, a first-order Taylor expansion of the failure criterion is given as

$$f_i^1 = f_i^0 + \left(\frac{\partial f_i^0}{\partial \underline{\sigma}^0}\right)^{\mathrm{T}} \Delta\underline{\sigma}^0 + \sum_{j=1}^{3} \left(\frac{\partial f_i^0}{\partial \hat{\varepsilon}_{pj}^0} \Delta\hat{\varepsilon}_{pj}^0\right) = 0, \tag{18}$$

where superscripts "0" and "1" indicate current and next iteration, respectively, and the subscript indicates the failure criterion ($i = 1, 2, 3$).

The stress increments in the current iteration are defined as

$$\Delta\underline{\sigma}^0 = \underline{D}(\Delta\underline{\varepsilon}_e^0) = \underline{D}(\Delta\underline{\varepsilon}^0 - \Delta\underline{\varepsilon}_p^0) = \underline{D}\left(\Delta\underline{\varepsilon}^0 - \sum_{i=1}^{3} \Delta\underline{\varepsilon}_{pi}^0\right) = \underline{D}\left[\Delta\underline{\varepsilon}^0 - \sum_{i=1}^{3} \left(\frac{\partial g_i^0}{\partial \underline{\sigma}^0} \Delta\lambda_i^0\right)\right]. \tag{19}$$

Since elastically predicted stresses are developed only in the initial iteration of each load step, $\Delta\underline{\varepsilon}^0 = 0$ in the subsequent iterations. The plastic strain rate multiplier can be obtained by inserting Eq. (19) into Eq. (18).

$$\underline{A}\Delta\underline{\lambda}^0 = \underline{F}^0, \tag{20}$$

where $A_{ij} = \left(\frac{\partial f_i^0}{\partial \underline{\sigma}^0}\right)^{\mathrm{T}} \underline{D}\left(\frac{\partial g_j^0}{\partial \underline{\sigma}^0}\right) + \left(\frac{\partial f_i^0}{\partial \hat{\varepsilon}_{pj}^0}\right) C_j$, $\Delta\underline{\lambda}^0 = \langle\, \Delta\lambda_1^0 \quad \Delta\lambda_2^0 \quad \Delta\lambda_3^0 \,\rangle^{\mathrm{T}}$, and $\underline{F} = \langle\, f_1^0 \quad f_2^0 \quad f_3^0 \,\rangle^{\mathrm{T}}$.

Using Eq. (20), the plastic strain multiplier for each failure criterion can be obtained. Then, stresses and equivalent plastic strains in the next iteration can be calculated.

$$\underline{\sigma}^1 = \underline{\sigma}^0 - \sum_{i=1}^{3} (\underline{D}\Delta\varepsilon_{pi}^0) = \underline{\sigma}^0 - \sum_{i=1}^{3} \left[\underline{D}\left(\frac{\partial g_i^0}{\partial \underline{\sigma}^0}\right)\Delta\lambda_i^0\right]. \tag{21}$$

$$\hat{\varepsilon}_{pi}^1 = \hat{\varepsilon}_{pi}^0 + C_i \Delta\lambda_i^0. \tag{22}$$

Through the iterative procedure in Eqs. (18)–(22), the stresses elastically predicted in the initial iteration of each load step are relaxed by the development of plastic strains. If the failure criteria in Eq. (18) updated with the new stress components are not satisfied, this relaxation procedure is applied again.

For fast and stable convergence in nonlinear calculations, the tangent stiffness matrix needs to be consistent with the iterative procedure mentioned. The tangent stiffness matrix for each iterative step can be obtained by differentiating Eqs. (18)–(22). Stress components in Eq. (19) are differentiated as:

$$\dot{\underline{\sigma}} = \underline{D}\dot{\underline{\varepsilon}} - \sum_{i=1}^{3}\left[\dot{\lambda}_i \underline{D}\left(\frac{\partial g_i}{\partial \underline{\sigma}}\right)\right] - \sum_{i=1}^{3}\left[\Delta\lambda_i \underline{D}\left(\frac{\partial^2 g_i}{\partial \underline{\sigma}^2}\right)\dot{\underline{\sigma}}\right], \tag{23a}$$

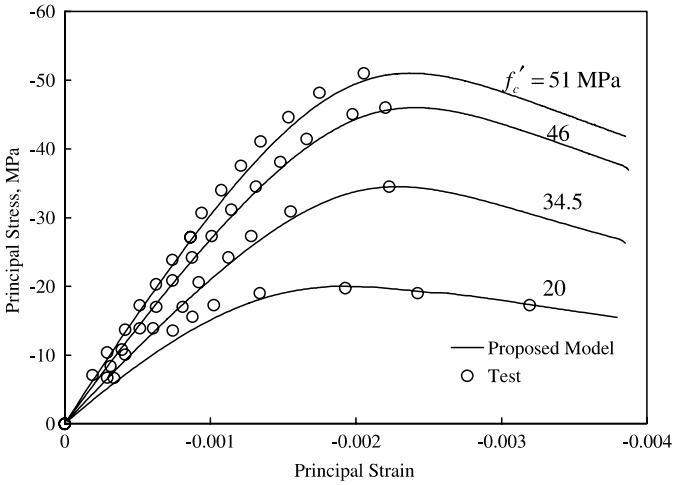


Fig. 8. Uniaxial test—Hognestad et al.

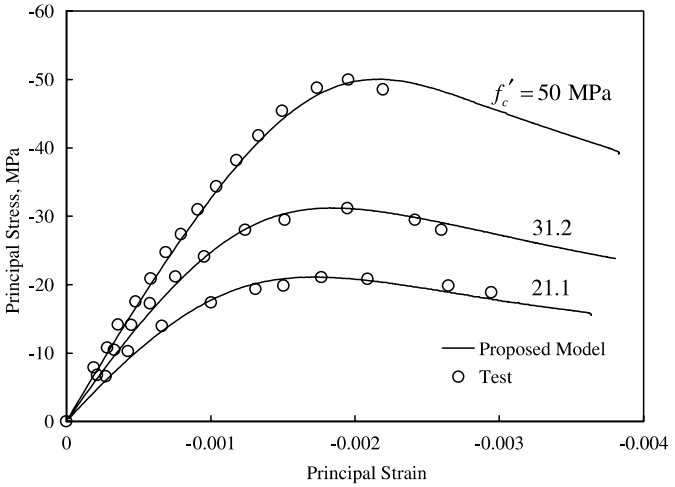


Fig. 9. Uniaxial test—Desayi and Krishnan.

and

$$\dot{\underline{\sigma}} = \left\{ \underline{I} + \sum_{i=1}^{3} \left[ \Delta\lambda_i \underline{D} \left( \frac{\partial^2 g_i}{\partial \underline{\sigma}^2} \right) \right] \right\}^{-1} \underline{D} \left[ \dot{\underline{\varepsilon}} - \sum_{i=1}^{3} \left( \dot{\lambda}_i \frac{\partial g_i}{\partial \underline{\sigma}} \right) \right] = \underline{R} \left[ \dot{\underline{\varepsilon}} - \sum_{i=1}^{3} \left( \dot{\lambda}_i \frac{\partial g_i}{\partial \underline{\sigma}} \right) \right]. \tag{23b}$$

To satisfy the consistency condition, the expansion in Eq. (18) should be eliminated.

$$\dot{f}_i = \left( \frac{\partial f_i}{\partial \underline{\sigma}} \right)^{\mathrm{T}} \dot{\underline{\sigma}} + \sum_{j=1}^{3} \left( \frac{\partial f_i}{\partial \hat{\varepsilon}_{\mathrm{p}j}} \dot{\hat{\varepsilon}}_{\mathrm{p}j} \right) = 0. \tag{24}$$

Using Eqs. (23) and (24),

$$\underline{B}\dot{\underline{\lambda}} = \underline{a}^{\mathrm{T}} \underline{R} \dot{\underline{\varepsilon}}, \tag{25}$$

where $B_{ij} = \left( \frac{\partial f_i}{\partial \underline{\sigma}} \right)^{\mathrm{T}} \underline{R} \left( \frac{\partial g_j}{\partial \underline{\sigma}} \right) + \left( \frac{\partial f_i}{\partial \hat{\varepsilon}_{\mathrm{p}j}} \right) C_j$, $\dot{\underline{\lambda}} = \langle \dot{\lambda}_1 \quad \dot{\lambda}_2 \quad \dot{\lambda}_3 \rangle^{\mathrm{T}}$, and $\underline{a} = \left\langle \frac{\partial f_1}{\partial \underline{\sigma}} \quad \frac{\partial f_2}{\partial \underline{\sigma}} \quad \frac{\partial f_3}{\partial \underline{\sigma}} \right\rangle$.

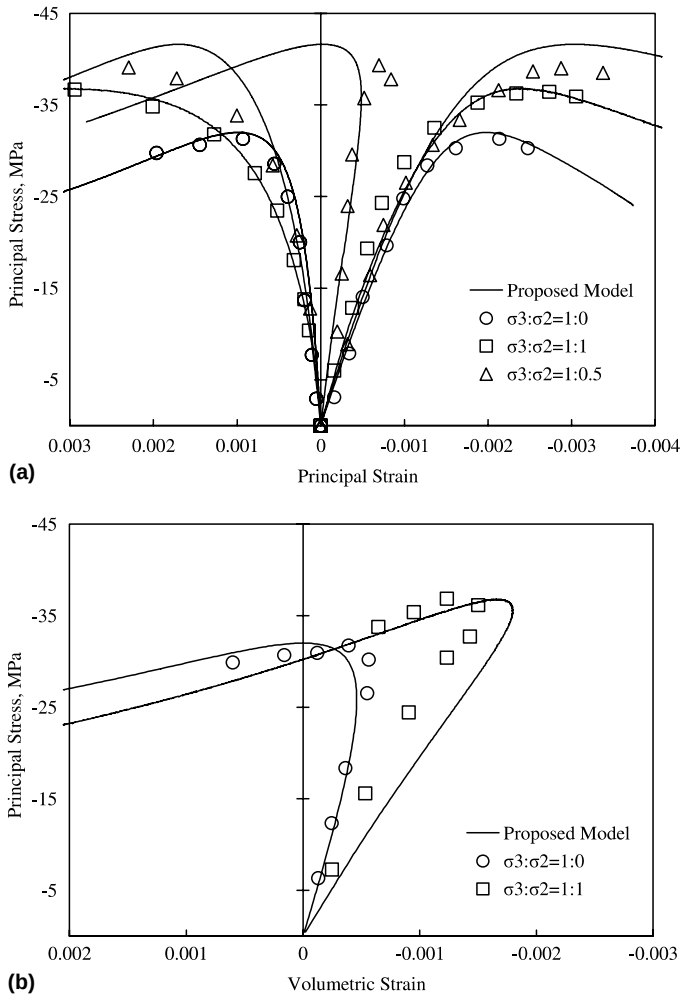


Fig. 10. Uniaxial and biaxial test—Kupfer et al.: (a) principal strain–principal stress; and (b) volumetric strain–principal stress.

From (23) and (25), the consistent tangent matrix can be derived as

$$\underline{D}_T = \underline{R} - \underline{RaB}^{-1}\underline{a}^{\mathrm{T}}\underline{R}^{\mathrm{T}}. \tag{26}$$

## 7. Verification

For verification, the numerical results obtained by the proposed model were compared with existing test results for various stress states and material properties. The numerical results on the uniaxial compressive behavior of concrete with various compressive strengths and elastic moduli, were compared with the test results by Hognestad et al. (1955) and Desayi and Krishnan (1964). In the test by Hognestad et al. (1955), $f'_c = 20$, 34.5, 46, and 51 MPa and $E_c = 18{,}700$, 21,550, 26,900, and 31,600 MPa. In the test by zDesayi and Krishnan (1964), $f'_c = 21.1$, 31.2, and 50 MPa and $E_c = 25{,}000$, 32,000, and 35,700 MPa.

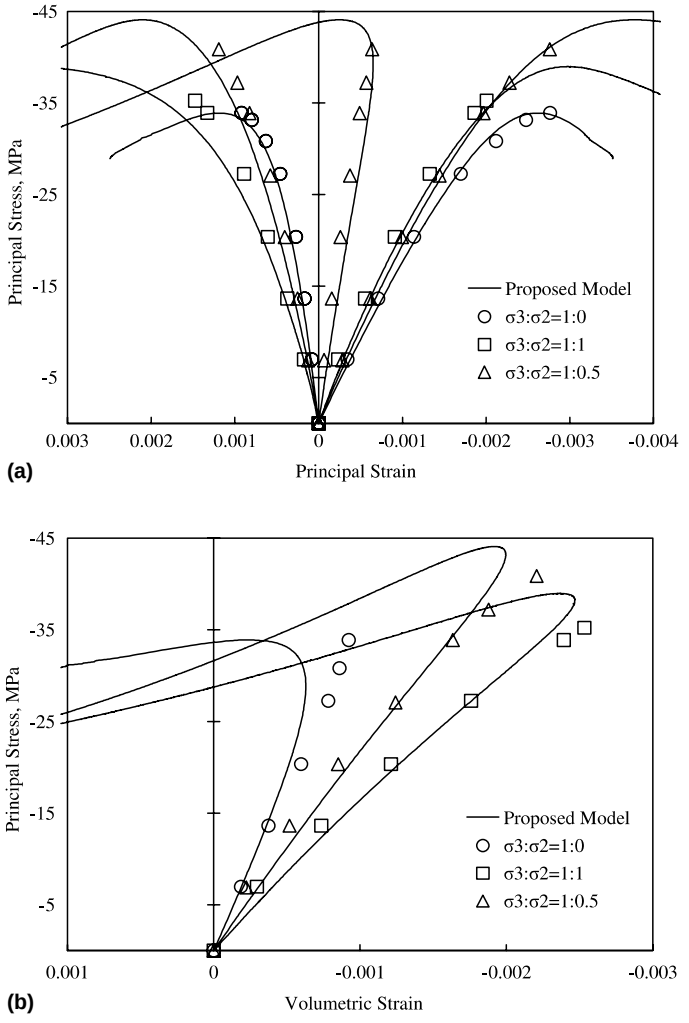


Fig. 11. Uniaxial and biaxial test—Tasuji et al.: (a) principal strain–principal stress; and (b) volumetric strain–principal stress.

The comparisons of the numerical and test results are shown in Figs. 8 and 9. As shown in the figures, the proposed model accurately described the uniaxial compressive behavior of concrete with various compressive strengths and elastic moduli. In the figures, post-peak stresses decreased more rapidly for higher strength concrete. Unlike existing plasticity models describing the post-peak behavior by using additional strain-softening variables, the proposed model can accurately describe such behavior without arbitrary adjustment of coefficients.

Figs. 10 and 11 show the stress–strain relations obtained from uniaxial and biaxial compression tests by Kupfer et al. (1969) and Tasuji et al. (1978). In the tests, $\sigma_2/\sigma_3 = 0,\ 0.5,\ 1$. In Kupfer et al. (1969), $f'_c = 32\,\text{MPa}$ and $E_c = 29{,}000\,\text{MPa}$. In Tasuji et al. (1978), $f'_c = 33.9\,\text{MPa}$ and $E_c = 19{,}600\,\text{MPa}$. Fig. 10(a) and Fig. 11(a) show the relations between principal strain and maximum principal stress, and

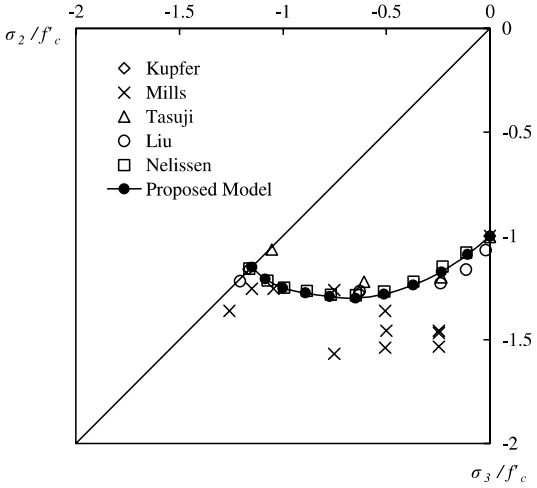


Fig. 12. Comparison with biaxial tests.

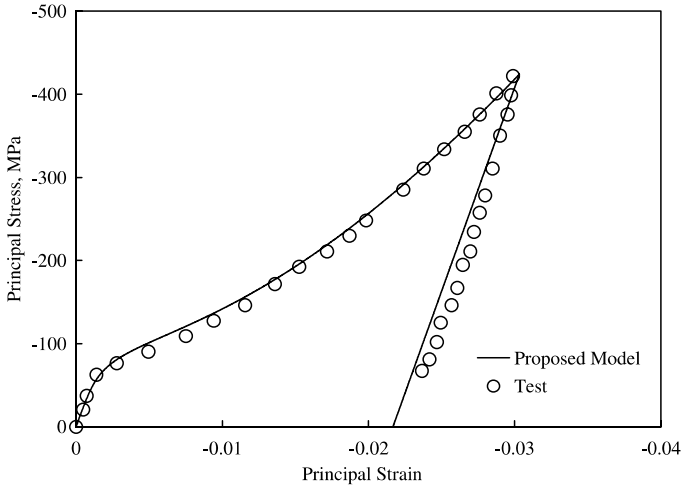


Fig. 13. Hydrostatic triaxial test—Green and Swanson ($f'_c = 48.4\,\text{MPa}$).

Fig. 10(b) and Fig. 11(b) show the relations between volumetric strain and maximum principal stress. As shown in Figs. 10 and 11, the proposed model accurately described the volumetric strain–principal stress relations as well as the principal strain–principal stress relations.

Fig. 12 shows the variations in the biaxial compressive strength according to the stress ratio $\sigma_2/\sigma_3$ (Kupfer et al., 1969; Mills and Zimmerman, 1970; Liu et al., 1972; Nelissen, 1972; Tasuji et al., 1978). The proposed model agrees well with the compressive strength of the biaxial compression tests except Mills and Zimmerman (1970).

Figs. 13 and 14 show the results of the hydrostatic triaxial compression tests by Green and Swanson (1973) and Kotsovos and Newman (1978) ($\sigma_1 = \sigma_2 = \sigma_3 < 0$). In Green and Swanson (1973), $f'_c = 48.4$ MPa and $E_c = 35{,}163$ MPa. In Kotsovos and Newman (1978), $f'_c = 31.7$ MPa and $E_c = 30{,}250$ MPa. The test results show the variations of the tangent stiffness with hydrostatic stress, which was described well by

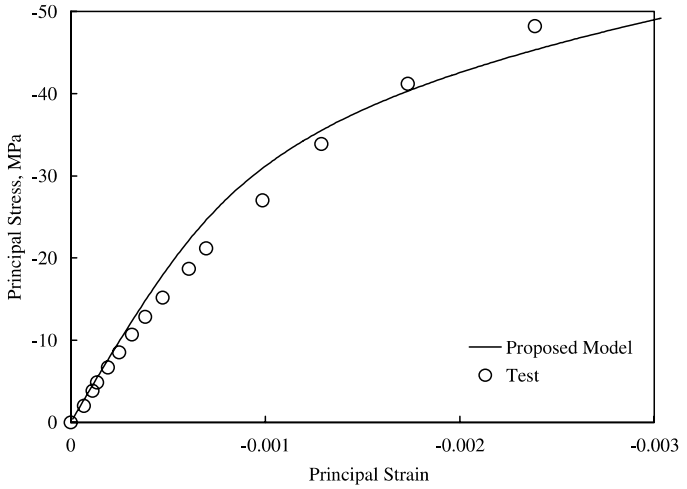


Fig. 14. Hydrostatic triaxial test—Kotsovos and Newman ($f'_c = 31.7$ MPa).

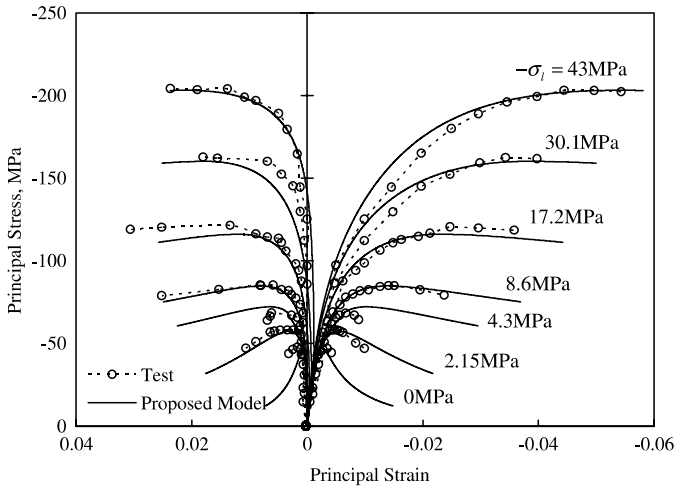


Fig. 15. Laterally confined triaxial test—Imran and Pantazopoulou ($f'_c = 47.4$ MPa).

the proposed model. This verifies accuracy of the volumetric stress–strain relation in Fig. 5(a), given by Bazant and Prat (1988b).

Figs. 15–18 show the results of laterally confined triaxial compression tests ($\sigma_3 < \sigma_2 = \sigma_1(=\sigma_l) < 0$). Fig. 15 shows the test results by Imran and Pantazopoulou (1996), where $f'_c = 47.4\,\text{MPa}$ and $E_c = 30{,}000\,\text{MPa}$. Figs. 16 and 17 show the test results by Kotsovos and Newman (1978), where $f'_c = 31.7\,\text{MPa}$ and $E_c = 30{,}250\,\text{MPa}$, and $f'_c = 46.9\,\text{MPa}$ and $E_c = 32{,}000\,\text{MPa}$, respectively. Fig. 18 shows the test results by Li and Ansari (1999), where $f'_c = 47.23\,\text{MPa}$ and $E_c = 40680.5\,\text{MPa}$. The test results showed the variations in the principal strain–principal stress relations for a wide range of lateral confining stress ($\sigma_l = 0.05$–$1.5f'_c$). As shown in the figures, the proposed model describes well the strength and ductility enhanced by the lateral confinement. Various laterally confined triaxial compression tests including the tests mentioned were

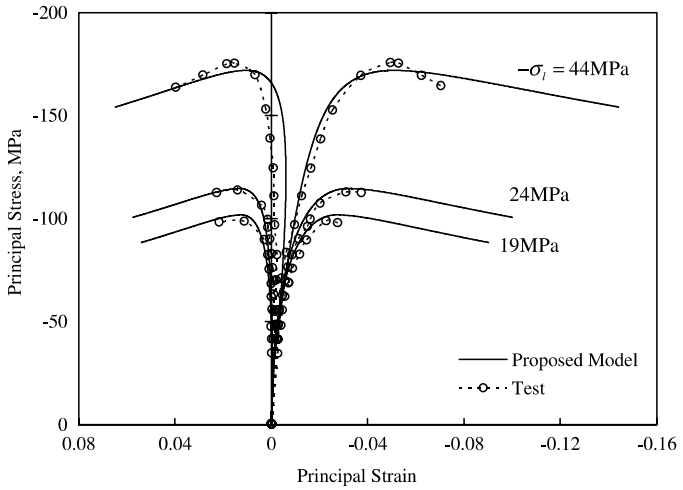


Fig. 16. Laterally confined triaxial test—Kotsovos and Newman ($f'_c = 31.7\,\text{MPa}$).

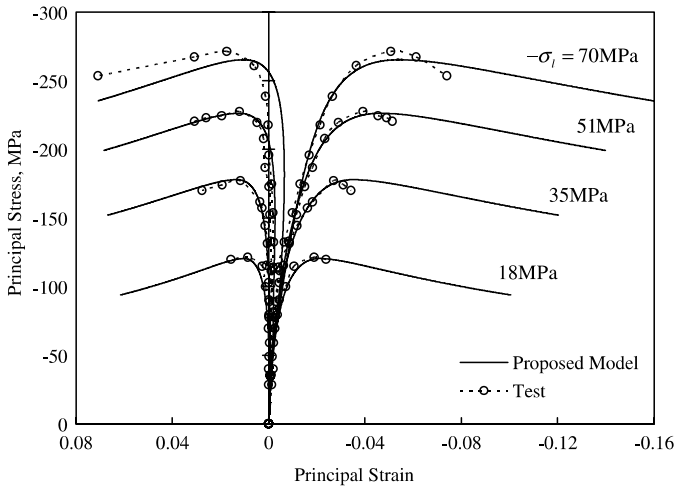


Fig. 17. Laterally confined triaxial test—Kotsovos and Newman ($f'_c = 46.9\,\text{MPa}$).

compared in Fig. 19. The figure demonstrates the accuracy of the proposed model. Particularly, the proposed model can accurately predict the enhanced compressive strength for mid- and low-strength concrete ($f'_c < 60$ MPa). For high-strength concrete ($f'_c \geqslant 60$ MPa), the compressive strength tends to be underestimated because the volumetric failure surface in Eq. (6a) does not accurately predict the volumetric plastic strain due to the overestimation of elastic modulus for high-strength concrete.

To verify the proposed model for the proportionally increasing triaxial compression, the numerical results were compared with the test results by van Mier (1986). Fig. 20 shows the principal strain–principal stress relations and volumetric strain–principal stress relations. The proposed model presented well the enhanced strength in triaxial compression. However, the proposed model overestimates the ductility and dilatancy of concrete. Fig. 21 shows the variations of the triaxial compressive strength with the magnitude of the hydrostatic stress in the deviatoric plane. The results given by the proposed model agreed with the

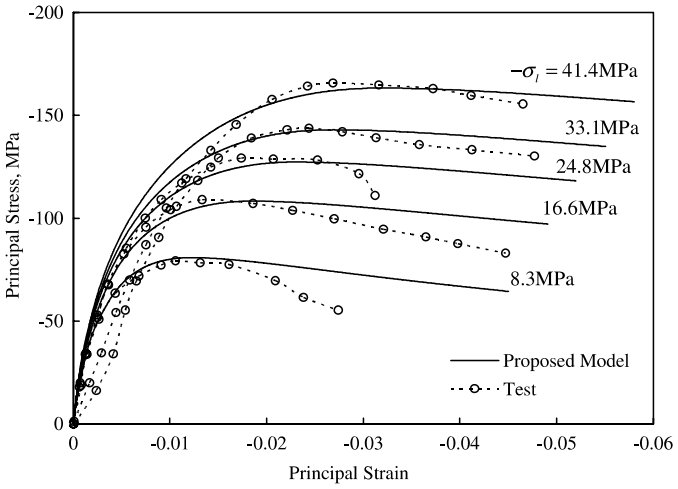


Fig. 18. Laterally confined triaxial test—Li and Ansari ($f'_c = 47.23$ MPa).

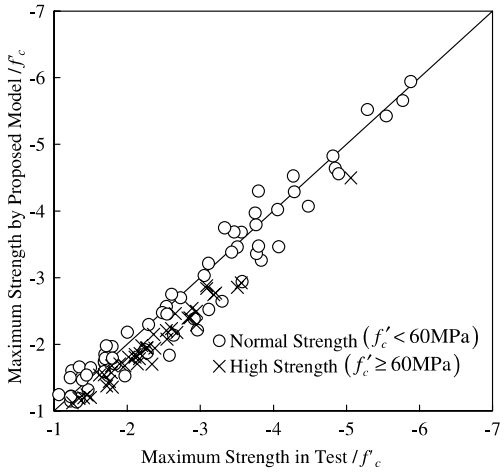


Fig. 19. Comparison with laterally confined triaxial tests.

test results by Launay and Gachon (1972) and the 5-parameter Willam–Warnke failure surface, which has been thought to accurately represent the strength enhancement in triaxial compression (Chen, 1982).

As shown in Figs. 8–21, generally, the proposed model predicted well the overall behavior of concrete in various stress states. However, the proposed model needs to be improved in several aspects. The proposed model tends to overestimate the post-peak strength and describe more ductile behavior than the test results. To describe the brittle post-peak behavior of concrete, slope of the descending branch of the deviatoric failure surface functions in Fig. 5(b) and (c) must be adjusted. In the proposed model, a single exponential equation originally proposed by Bazant and Prat (1988b) was used to present both pre- and post-peak failure surface. Therefore, to more accurately describe the post-peak behavior, the post-peak failure surface function must be separated from the pre-peak failure surface function.

Also, to accurately predict maximum strength of the high strength concrete in Fig. 19, the equation of the elastic modulus defined as a function of the concrete strength ($E_c = 4730\sqrt{f'_c}$(MPa)) needs to be

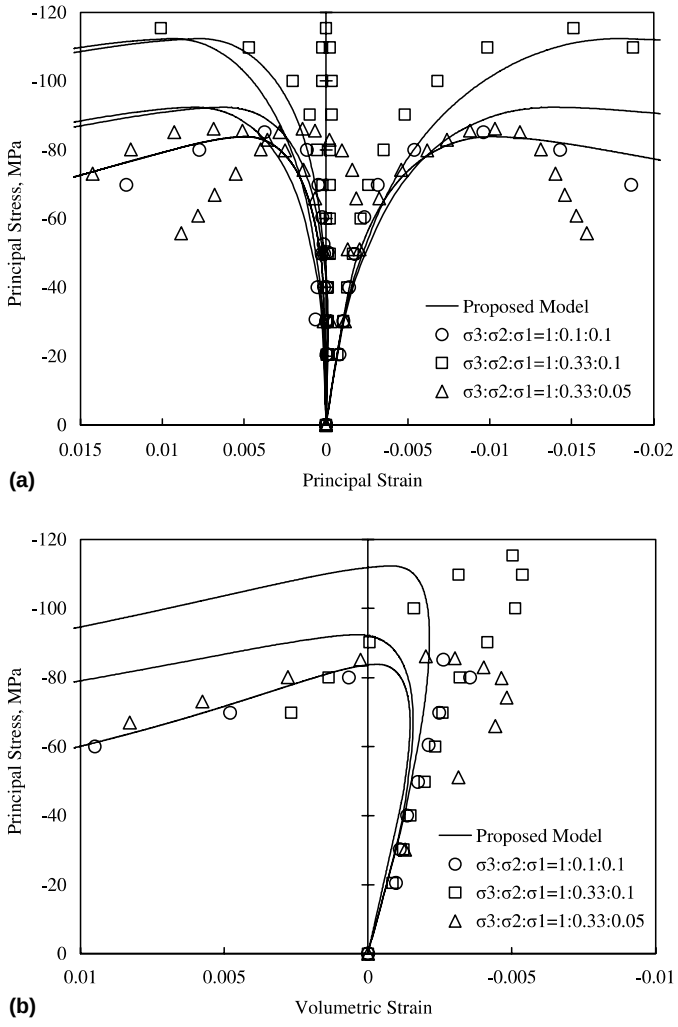


Fig. 20. Triaxial test—van Mier: (a) principal strain–principal stress; and (b) volumetric strain–principal stress.

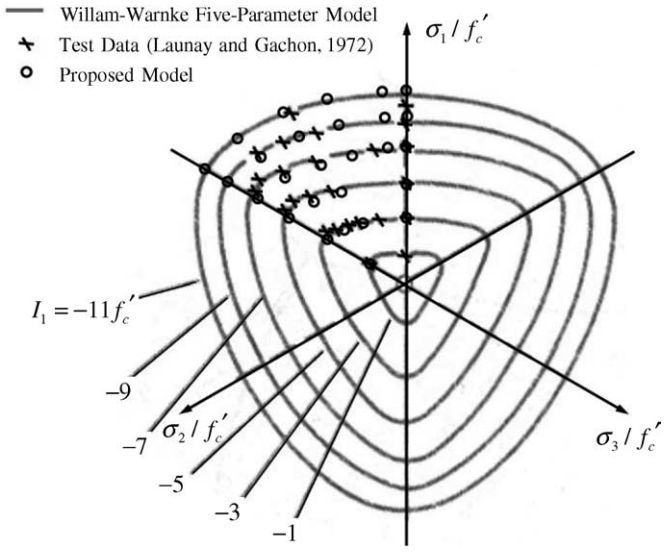


Fig. 21. Comparison with triaxial test (Launay and Gachon) and Willam–Warnke 5-parameter model.

improved to be applicable to the high strength concrete. In the proportionally increasing triaxial test shown in Fig. 20, the proposed model overestimated dilatancy of the concrete. This results indicate that the coefficient $\kappa$ ($= -J_2/I_1^2$) used in Eqs. (15b) and (15c) to define the plastic potentials needs to be defined by various parameters including $I_1$, $J_2$, and $J_3$.

## 8. Conclusions

A plasticity model using a new approach in defining the failure criteria was developed to describe the nonlinear behavior of concrete in various compressive stress states. In the proposed model, a stress was decomposed into three orthogonal components representing volumetric and deviatoric behavioral characteristics, respectively. Three failure criteria were provided independently for the each stress component. For this, the plasticity model using multiple failure criteria was implemented. Unlike existing plasticity models using a single failure surface, the proposed model uses three independent failure surfaces, which allows the behavioral characteristics of concrete in various stress states to be described more accurately. To present dilatancy due to compressive damage, a simple non-associative flow rule was proposed.

The proposed model was verified by comparisons of its results with those of existing uni-, bi-, and triaxial tests. The comparisons show that the proposed model is applicable to general use because it can predict most of the test results, using basic material properties such as uniaxial compressive strength and elastic modulus.

## Acknowledgment

This research was financially supported by the Ministry of Construction and Transportation of Korea (04 Core Technology C02-02) and the Korea Earthquake Engineering Research Center, and the authors are grateful to the authorities for their support.

## References


Bazant, Z.P., Prat, P.C., 1988a. Microplane model for brittle–plastic material: I. Theory. Journal of Engineering Mechanics. ASCE 114 (10), 1672–1688.

Bazant, Z.P., Prat, P.C., 1988b. Microplane model for brittle–plastic material: II. Verification. Journal of Engineering Mechanics. ASCE 114 (10), 1689–1702.

Bellotti, R., Rossi, P., 1991. Cylinder tests: experimental technique and results. Materials and Structures. RILEM 24, 45–51.

Chen, A.C.T., Chen, W.F., 1975. Constitutive Relations for Concrete. Journal of Engineering Mechanics, ASCE 101 (4), 465–481.

Chen, W.F., 1982. Plasticity in Reinforced Concrete. McGraw-Hill Book Company, New York.

Crisfield, M.A., 1991Non-linear Finite Element Analysis of Solids and Structures, vol. 1. John Wiley & Sons Inc., New York.

Desayi, P., Krishnan, P., 1964. Equation for stress–strain curves of concrete. ACI Journal 61, 345–350.

Grassl, P., Lungren, K., Gylltoft, K., 2002. Concrete in compression: a plasticity theory with a novel hardening law. International Journal of Solids and Structures 39 (20), 5205–5223.

Green, S.J., Swanson, S.R., 1973. Static constitutive relations for concrete. In: Air Force Weapons Lab. Tech. Rep., AFWL-TR-72-244, Kirtland Air Force Base, Albuquerque, N. Mex.

Hognestad, E., Hanson, N.W., McHenry, D., 1955. Concrete stress distribution in ultimate strength design. ACI Journal 52, 455–477.

Imran, I., Pantazopoulou, S.J., 1996. Experimental study of plain concrete under triaxial stress. ACI Materials Journal 93 (6), 589–601.

Imran, I., Pantazopoulou, S.J., 2001. Plasticity model for concrete under triaxial compression. Journal of Engineering Mechanics. ASCE 127 (3), 281–290.

Kang, H., Willam, K., 1999. Localization characteristics of triaxial concrete model. Journal of Engineering Mechanics. ASCE 125 (8), 941–950.

Kotsovos, M.D., Newman, J.B., 1978. Generalized stress–strain relations for concrete. Journal of Engineering Mechanics Division. ASCE 104 (4), 845–856.

Kupfer, H.B., Hildorf, H.K., Rusch, H., 1969. Behavior of concrete under biaxial stresses. ACI Journal 66 (8), 656–666.

Launay, P., Gachon, H., 1972. Strain and ultimate strength of concrete under triaxial stress. Paper 13. ACI Special Publication-34.

Li, Q., Ansari, F., 1999. Mechanics of damage and constitutive relationships for high-strength concrete in triaxial compression. Journal of Engineering Mechanics. ASCE 125 (1), 1–10.

Liu, T.C.Y., Nilson, A.H., Slate, F.O., 1972. Stress–strain response and fracture of concrete in uniaxial and biaxial compression. ACI Journal 69 (5), 291–295.

Menetrey, P., Willam, K., 1995. Triaxial failure criterion for concrete and its generalization. ACI Structural Journal 92 (3), 311–318.

Mills, L.L., Zimmerman, R.M., 1970. Compressive strength of plain concrete under multiaxial loading conditions. ACI Journal 67 (10), 802–807.

Nelissen, L.J.M., 1972. Biaxial testing of normal concrete. Heron 18 (1).

Park, H., Klingner, R.E., 1997. Nonlinear analysis of RC members using plasticity with multiple failure criteria. Journal of Structural Engineering. ASCE 123 (5), 643–651.

Pramono, E., Willam, K., 1989. Fracture energy-based plasticity formulation of plain concrete. Journal of Engineering Mechanics. ASCE 115 (6), 1183–1204.

Sfer, D., Carol, I., Gettu, R., Etse, G., 2002. Study of the behavior of concrete under triaxial compression. Journal of Engineering Mechanics. ASCE 128 (2), 156–163.

Smith, S.S., Willam, K.J., Gerstle, K.K., Sture, S., 1989. Concrete over the top, or: is there life after peak. ACI Materials Journal 86 (5), 491–497.

Tasuji, M.E., Slate, F.O., Nilson, A.H., 1978. Stress–strain response and fracture of concrete in biaxial loading. ACI Journal 75 (7), 306–312.

van Mier, J.G.M., 1986. Multiaxial strain-softening of concrete. Materials and Structures. RILEM 19 (111), 179–200.

Wang, C.-Z., Guo, Z.-H., Zhang, X.-Q., 1987. Experimental investigation of biaxial and triaxial compressive strength. ACI Materials Journal 84 (2), 92–100.

Xie, J., Elwi, A.E., MacGregor, J.G., 1995. Mechanical properties of three high-strength concretes containing silica fume. ACI Materials Journal 92 (2), 135–145.